Atomic vibrational density of states in crystalline and amorphous $Tb_{1-x}Fe_x$ alloy thin films studied by nuclear resonant inelastic x-ray scattering (NRIXS)

2004 J. Phys.: Condens. Matter 16 S379

(http://iopscience.iop.org/0953-8984/16/5/004)

INSTITUTE OF PHYSICS PUBLISHING JOURNAL OF PHYSICS: CONDENSED MATTER

J. Phys.: Condens. Matter **16** (2004) S379–S393 PII: S0953-8984(04)65140-X

Atomic vibrational density of states in crystalline and amorphous $Tb_{1-x}Fe_x$ alloy thin films studied by nuclear resonant inelastic x-ray scattering (NRIXS)

W Keune[1,4], T Ruckert[1], B Sahoo[1], W Sturhahn[2], T S Toellner[2], E E Alp[2] and R Röhlsberger[3]

[1] Institut für Physik, Universität Duisburg-Essen, D-47048 Duisburg, Germany
[2] Advanced Photon Source, Argonne National Laboratory, Argonne, IL 60439, USA
[3] Fachbereich Physik, Universität Rostock, D-18055 Rostock, Germany

E-mail: keune@uni-duisburg.de

Received 24 June 2003
Published 23 January 2004
Online at stacks.iop.org/JPhysCM/16/S379 (DOI: 10.1088/0953-8984/16/5/004)

Abstract

Nuclear resonant inelastic x-ray scattering of 14.4125 keV synchrotron radiation was employed to measure directly the partial (Fe projected) vibrational density of states (VDOS), $g(E)$, of vapour-quenched amorphous (a-)$Tb_{1-x}{}^{57}Fe_x$ thin film alloys ($0.20 \leqslant x \leqslant 0.82$) and epitaxial $Tb^{57}Fe_2(110)$ thin films. A comparison of the VDOS measured at 300 and 10 K, respectively, demonstrates that the vibrational anharmonicity is small in these systems. The probability of recoilless absorption (f factor), the average kinetic energy per Fe atom and the average force constant were obtained. A plot of $g(E)/E^2$ versus E proves the existence of non-Debye-like vibrational excitations at excitation energies below about 10 meV for the amorphous alloys. At a constant film thickness of 17.5 nm, the probability of these excitations scales about linearly with the Tb concentration.

(Some figures in this article are in colour only in the electronic version)

1. Introduction

Nuclear resonant inelastic x-ray scattering (NRIXS) of 14.4125 keV synchrotron radiation by ^{57}Fe nuclei [1–3] is a powerful method to explore the atomic vibrational properties of condensed matter not available otherwise [4, 5]. NRIXS allows the direct measurement of the frequency distribution of atomic vibrations, i.e. the vibrational density of states (VDOS), $g(E)$, for the vibrating resonant isotope in the crystalline or amorphous state. This resonant isotope projected 'partial' VDOS is a key quantity from which important thermodynamic properties

[4] Author to whom any correspondence should be addressed.

may be deduced [5]. NRIXS has opened the domain of lattice dynamics in thin film, interface and multilayer research [6–10].

In the present investigation (which is a continuation of our earlier work [11]) the Fe-projected VDOS of vapour-quenched amorphous (a-)$Tb_{1-x}{}^{57}Fe_x$ thin film alloys and, for comparison, of an epitaxial $Tb^{57}Fe_2(110)$ thin film with the cubic Laves phase structure was measured by NRIXS. Amorphous systems are of considerable interest because of their anomalous behaviour in the low-energy part of the VDOS [12]. In particular, the appearance of the so-called 'boson peak' in the reduced VDOS, $g(E)/E^2$, as an excess contribution in comparison with the usual Debye law, ($g(E)/E^2 =$ constant), is a subject of continuous interest [13–16]. Earlier results obtained by coherent inelastic neutron scattering on bulk samples of binary metallic glasses, such as $Mg_{70}Zn_{30}$ [16], provided evidence of an enhancement of the VDOS at low excitation energies as compared to the Debye behaviour. In the present work we present a systematic study of $g(E)/E^2$ of a-$Tb_{1-x}Fe_x$ thin films over a wide concentration range. Vapour-quenched a-$Tb_{1-x}Fe_x$ alloy films with thicknesses between 175–800 Å have been found to be metastable at room temperature (RT) in the regime $0.20 \leqslant x \leqslant 0.82$ [11, 17–19]. Therefore, this is a suitable amorphous system for the study of the concentration dependence of vibrational properties.

2. Experimental procedures and sample preparation

The experiments were performed at the undulator beamline 3-ID of SRI-CAT at the Advanced Photon Source (APS). The bandwidth of the highly collimated beam of x-rays from the undulator is reduced to a value of the order of electronvolts by a high-heat-load monochromator that uses two symmetric diamond (111) Bragg reflections in a nondispersive arrangement. Further monochromatization down to 2.3 meV in bandwidth (FWHM) is achieved by a high-resolution nested Si crystal monochromator [20, 21]. The monochromatized synchrotron beam illuminated the ^{57}Fe-containing thin films under a grazing angle of ≈4 mrad. The energy was tuned in steps of 0.4 meV around the 14.4125 keV nuclear resonance of ^{57}Fe. An avalanche photodiode [22] was mounted above the thin film and detected the time-delayed characteristic 6.4 keV fluorescence x-rays of iron emitted after the nuclear de-excitation. The measurements were performed with the samples usually at RT, and in a few cases at 10 K. The collection times were 2–10 h per spectrum, depending on film thickness and Fe content. The NRIXS data evaluation and extraction of the VDOS was performed by using the computer program PHOENIX described elsewhere [23].

The a-$Tb_{1-x}{}^{57}Fe_x$ alloy thin films were prepared in ultrahigh vacuum (base pressure $\sim 5 \times 10^{-10}$ mbar) by thermal co-evaporation of Tb metal (99.99 at.% purity) and metallic ^{57}Fe (99.95 at.% purity, 95.5% enriched in ^{57}Fe) from independently computer-controlled Knudsen cells [17]. The pressure during evaporation was lower than 1×10^{-9} mbar. The deposition rates of Tb and ^{57}Fe were measured independently by two calibrated quartz-crystal oscillators and controlled by a personal computer. The desired alloy composition was achieved by selecting a constant ratio of the Tb and ^{57}Fe deposition rates, while maintaining the individual deposition rates constant. Depending on the alloy composition the deposition rates ranged between 0.01 and 0.70 Å s^{-1}. All alloy compositions, x, given here are the nominal compositions as determined from the ratio of the two deposition rates. The error in x is estimated to be ± 0.01. The alloy film thickness, t, was usually 17.5 nm for the Fe-rich films, and was increased up to 80.0 nm for the Fe-poor samples in order to optimize the NRIXS measurement time. The amorphous films were grown at 300 K on oxidized Si(001) wafers that were usually initially coated by a 20.0 nm thick polycrystalline Pt buffer layer. Reflection of the synchrotron beam at the Pt layer in grazing incidence enhances the 6.4 keV fluorescence signal of inelastic nuclear

Table 1. Survey of the different a-$Tb_{1-x}{}^{57}Fe_x$ alloy thin films and their thicknesses.

Composition x	Film thickness (nm)
0.20	72.0
0.25	54.7
0.30	80.0
0.30	17.5
0.33	38.9
0.35	36.1
0.37	33.6
0.44	26.6
0.50	22.2
0.60	17.5
0.67	17.5
0.77	17.5
0.82	80.0
0.82	17.5

resonance absorption in 17.5 nm thick a-$Tb_{1-x}{}^{57}Fe_x$ overlayers due to a waveguide effect (GIAR effect) [24]. All samples were coated with a 5–10 nm thick Si layer for protection. A survey of all a-$Tb_{1-x}{}^{57}Fe_x$ samples and their thicknesses is given in table 1.

For comparison we have also prepared a 80.0 nm thick crystalline $Tb^{57}Fe_2(110)$ thin film with the cubic Laves phase structure by molecular beam epitaxy according to the procedure reported in [25]. This film was grown at $\sim$500 °C by co-deposition of Tb and ^{57}Fe with the appropriate ratio of deposition rates on a (sapphire)$Al_2O_3(11\bar{2}0)$ substrate which carried a 35.0 nm thick Nb(110) buffer layer and a 1.5 nm thick ^{57}Fe seed layer on the Nb surface. The $Tb^{57}Fe_2(110)$ film was coated by 5 nm Si for protection.

3. Sample characterization

The crystallographic structure of the samples was characterized by (θ–2θ) x-ray diffraction (XRD) and ^{57}Fe conversion electron Mössbauer spectroscopy (CEMS). Cu Kα-radiation and a graphite monochromator were used for XRD. CEM spectra were taken at RT by using a conventional He–CH_4 proportional counter with the film surface perpendicular to the incident 14.4 keV γ-ray of the ^{57}Co (Rh matrix) source. The CEM spectra were least-squares fitted by using the NORMOS computer program by Brand [26].

Figure 1 exhibits the XRD pattern of the epitaxial $Tb^{57}Fe_2(110)$ film (top) and the a-$Tb_{0.33}{}^{57}Fe_{0.67}$ film (bottom). Both samples have the same composition, x. Figure 1 confirms the (110)-epitaxial orientation of the $Tb^{57}Fe_2$ film, since only (220) and (440) Bragg reflections are observed. In the case of the a-$Tb_{0.33}{}^{57}Fe_{0.67}$ film, only Bragg peaks of the polycrystalline Pt buffer layer and no Bragg reflections of the Tb–Fe film are observed, confirming its amorphous structure. The amorphous structure of all other a-$Tb_{1-x}{}^{57}Fe_x$ films was further confirmed by XRD [11].

The CEM spectra (figure 2) are in agreement with the XRD results. The CEM spectrum of epitaxial $Tb^{57}Fe_2(110)$ (figure 2, top) exhibits sharp resonance lines typical for a well-ordered crystalline system. Although all the Fe sites in the cubic $TbFe_2$ Laves phase are chemically equivalent, this spectrum can be decomposed into two Zeeman-split sextets with sharp Lorentzian lines. They correspond to two locally different Fe sites ($i = 1, 2$) which are distinct in their different effective quadrupolar effects and dipolar hyperfine fields [27],

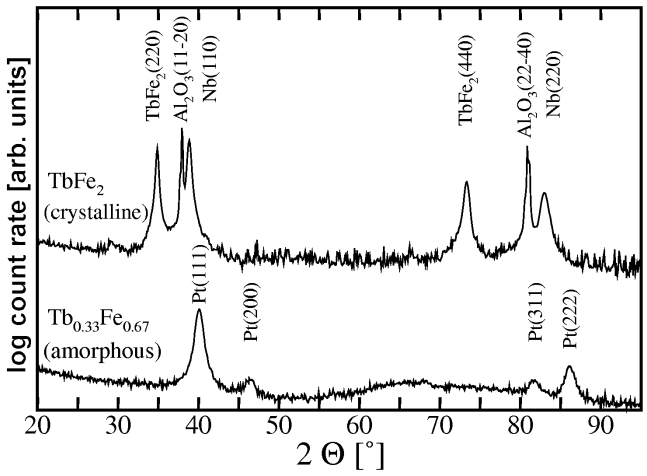

Figure 1. XRD patterns of 80 nm thick epitaxial $Tb^{57}Fe_2(110)$ film grown on a Nb(110) buffer layer on sapphire $Al_2O_3(11\bar{2}0)$ (top) and of 17.5 nm thick amorphous $Tb_{0.33}{}^{57}Fe_{0.67}$ alloy thin film grown on a Pt buffer layer on a Si wafer (bottom).

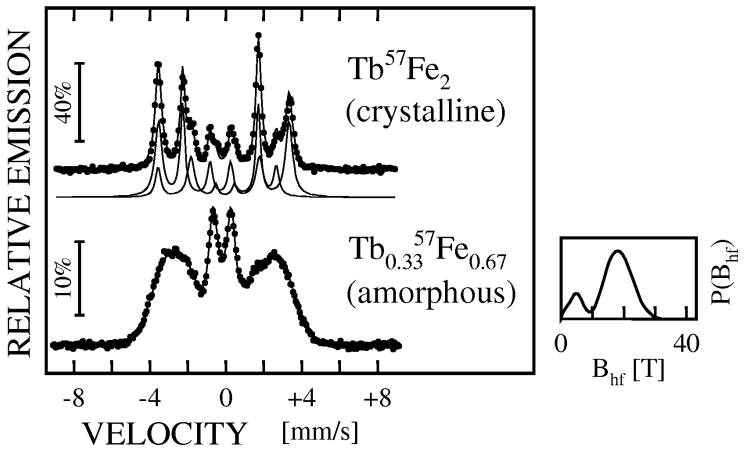

Figure 2. RT Mössbauer spectra of 80 nm thick epitaxial $Tb^{57}Fe_2(110)$ film (top) and 17.5 nm thick amorphous $Tb_{0.33}{}^{57}Fe_{0.67}$ film (bottom) with its hyperfine field distribution $P(B_{\rm hf})$ (right-hand side). The spectrum of epitaxial $Tb^{57}Fe_2$ was least-squares-fitted with two Zeeman sextets.

both being proportional to the angular factor $f(\theta_i) = 3\cos^2\theta_i - 1$. θ_1 defines the relative orientation of the magnetization direction (here closely aligned along the $[\bar{1}11]$ and $[\bar{1}1\bar{1}]$ in-plane directions) and the $\langle 111\rangle$ equivalent electric-field gradient directions [27]. The Mössbauer spectral parameters of these magnetically distinct Fe sites in $Tb^{57}Fe_2(110)$ obtained from least-squares fitting are given in table 2.

The CEM spectrum of the a-$Tb_{0.33}{}^{57}Fe_{0.67}$ film (figure 2, bottom) is similar to those reported earlier for a-$Tb_{1-x}{}^{57}Fe_x$ [11, 17–19, 28] and confirms the amorphous structure. These spectra have been analysed in terms of a broad distribution of hyperfine magnetic fields $P(B_{\rm hf})$ (figure 2, bottom), assuming a weak linear correlation between hyperfine field $B_{\rm hf}$ and the isomer shift δ. The average Fe spin direction is found to be preferentially perpendicular to the

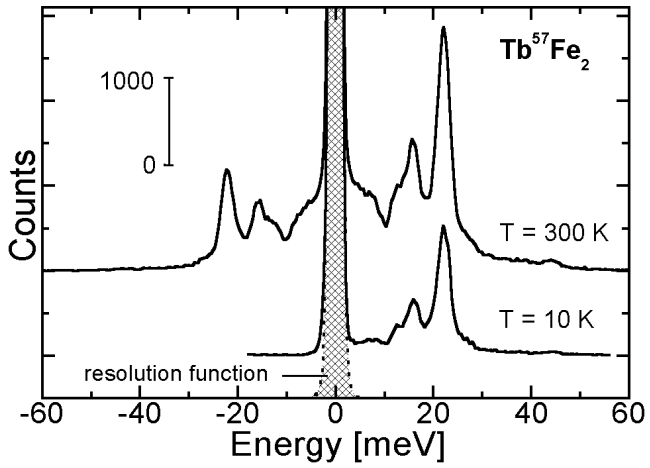

Figure 3. Intensity (number of counts) versus energy transfer to the lattice of 80 nm thick epitaxial $Tb^{57}Fe_2(110)$ film, measured at 300 K (top) and 10 K (bottom). Also shown is the instrumental resolution function with a FWHM of 2.3 meV (broken line with hatched area). (For clarity the spectra are vertically displaced.)

Table 2. Mössbauer spectral parameters of the two Fe sites in an epitaxial Tb ^{57}Fe(110) thin film (cubic Laves phase) at RT. B_{hf} = hyperfine magnetic field, δ = isomer shift (relative to α-Fe at RT), 2ε = quadrupole nuclear-level shift, $R_{2,3} = R_{5,4}$ = line intensity ratio of line no 2(5) and line no 3(4) of the sextet and area = relative spectral area (relative intensity) of the sextet.

Fe site	B_{hf} (T)	δ (mm s^{-1})	2ε (mm s^{-1})	$R_{2,3}$	Area (%)
#1	21.4	−0.090	+0.184	2.90	64
#2	19.2	−0.105	−0.356	3.70	36

film plane [11, 17–19, 28]. The Mössbauer spectral parameters of our a-$Tb_{1-x}{}^{57}Fe_x$ thin films are reported in [11, 17].

4. NRIXS results and discussion

4.1. Vibrational excitation probability and atomic vibrational parameters

Figure 3 exhibits typical NRIXS spectra (excitation probability versus energy transfer E to the lattice) of the epitaxial $Tb^{57}Fe_2(110)$ thin film (Laves phase) measured at RT (300 K) and 10 K, respectively. The spectra show a dominant central elastic peak at the nuclear transition energy E_0 (energy transfer $E = 0$ meV, i.e. the zero-phonon or 'Mössbauer' line) and side bands at lower and higher energy. X-rays with less energy than E_0 excite the nuclear resonance by net annihilation of vibrational quanta or phonons (low-energy side band). The high-energy side band originates from the creation of vibrational quanta or phonons. The observed asymmetry in the spectra reflects the 'detailed balance' [29] due to the Boltzmann factor. It is clear from the absence of the low-energy side band at 10 K that phonon annihilation is negligible at that temperature. The side bands in figure 3 show structure with sharp peaks which is a typical feature of crystalline solids. The instrumental resolution function with a full width at half-maximum (FWHM) of 2.3 meV is also depicted in figure 3. The resolution function is nearly symmetrical and falls off rapidly from the centre without having extended wings.

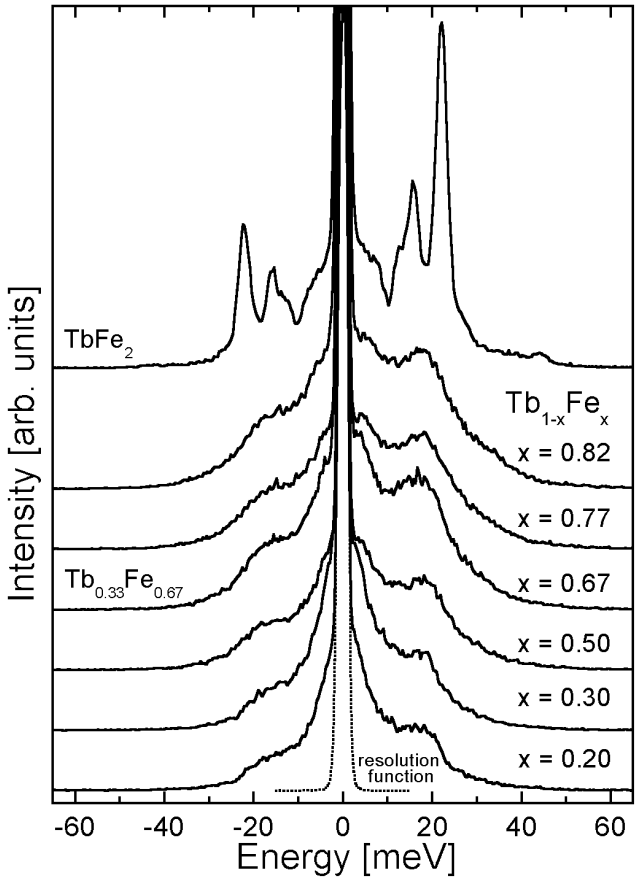

Figure 4. Intensity versus energy transfer obtained at 300 K from 80 nm thick epitaxial $Tb^{57}Fe_2(110)$ film (top) and from amorphous $Tb_{1-x}{}^{57}Fe_x$ films with $x = 0.20$ (72.0 nm thick), 0.30 (80.0 nm thick), 0.50 (22.2 nm thick), 0.67 (17.5 nm thick), 0.77 (17.5 nm thick) and 0.82 (80.0 nm thick) (from bottom to top). Also shown is the instrumental resolution function with a FWHM of 2.3 meV (dotted curve). (For clarity the spectra are vertically displaced.)

Figure 4 exhibits typical NRIXS spectra measured on a-$Tb_{1-x}{}^{57}Fe_x$ films at RT for different alloy compositions x. For comparison the 300 K NRIXS spectrum of the epitaxial $Tb^{57}Fe(110)$ film (figure 3) is shown again in figure 4 (top). One can observe that, contrary to the crystalline case, the vibrational side bands of the amorphous films have little structure and no sharp peaks, which is typical for the amorphous state [7].

After subtraction of the central elastic peak from the measured NRIXS spectra the data were normalized according to standard procedures [2, 5, 23], yielding the vibrational excitation probability per unit energy, $W(E)$. This normalization involves Lipkin's 'sum rule' [30–32] which states that the first-order moment of the normalized energy spectrum $W(E)$ is equal to the recoil energy, E_R, of the free ^{57}Fe atom, with $E_R = E_\gamma^2/2Mc^2$ ($E_\gamma =$ photon energy, $M =$ nuclear mass). As a typical example, the measured excitation probability density $W(E)$ of the epitaxial $Tb^{57}Fe(110)$ film is shown in figure 5 (open circles) on a logarithmic scale.

Several other moments of the excitation probability density $W(E)$ provide important model-independent quantities for the Fe atom in the solid [4, 5, 29]. The zero-order moment

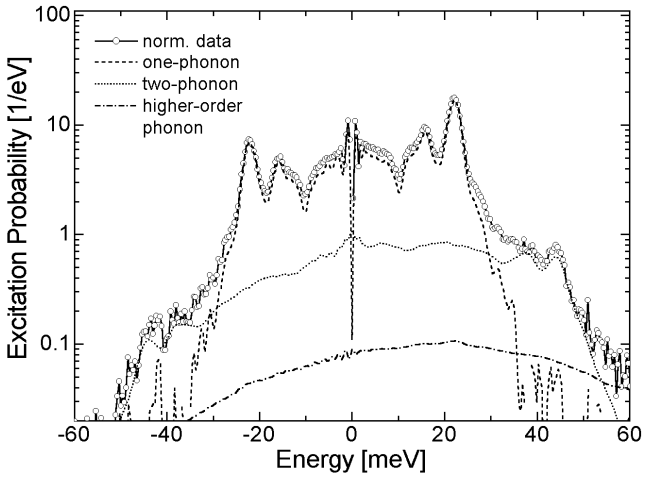

Figure 5. Total vibrational excitation probability density versus energy transfer to the lattice of epitaxial $Tb^{57}Fe_2$(110) thin film at 300 K versus energy transfer (open circles) and its decomposition into one-phonon (broken curve), two-phonon (dotted curve) and multi-phonon (chain curve) contributions.

gives $1 - f$, i.e. the Lamb–Mössbauer factor (f factor), the second-order moment gives the average kinetic energy and the third-order moment provides the average curvature of the potential energy, i.e. the average force constant. In figure 6 we show these moments versus the composition x of the a-$Tb_{1-x}{}^{57}Fe_x$ thin films. Values of the epitaxial $Tb^{57}Fe_2$ film are also given. The f factor (figure 6(a)) and the average force constant (figure 6(b)) increase with the Fe concentration x of the amorphous alloys. On the other hand, the average kinetic energy (figure 6(c)) is essentially constant in the range $0.20 \leqslant x \leqslant 0.67$ and seems to increase somewhat at higher Fe concentrations; we may assume similar behaviour of the average potential energy per Fe atom by virtue of the virial theorem. Near $x = 0.30$ fluctuations appear in the data of figures 6(a)–(c), which are possibly related to the fact that the thermodynamic phase diagram for crystalline Tb–Fe alloys shows a eutectic point in that regime [33], and small deviations of x might also strongly affect the amorphous state there. Compared with the amorphous alloys, the f factor of the epitaxial $Tb^{57}Fe_2$ film is found to be somewhat larger, while the other quantities are of similar magnitude. Figure 6 also demonstrates that these quantities essentially do not depend on the film thickness in the range 17.5–80.0 nm.

4.2. Partial vibrational density of states $g(E)$

The partial vibrational (or phonon) density of states, $g(E)$, was deduced from the measured vibrational excitation probability density, $W(E)$, according to standard procedures [2, 5, 23]. $W(E)$ is composed of contributions from one-phonon, two-phonon and multi-phonon scattering: $W(E) = S_1(E) + S_2(E) + S_3(E) + \cdots$. The explicit relationship between the one-phonon contribution, $S_1(E)$, and the single-phonon density of states, $g(E)$, is given by [5]

$$g(E) = \frac{3E}{E_R}\frac{S_1(E)}{f}(1 - e^{-E/K_B T}).$$

The mathematical procedure to extract $S_1(E), S_2(E), \ldots$ and $g(E)$ from the measured probability density $W(E)$ is described in detail elsewhere [2, 4, 23, 34, 35]. As an example, the one-phonon, two-phonon and the sum of higher-order phonon contributions for epitaxial

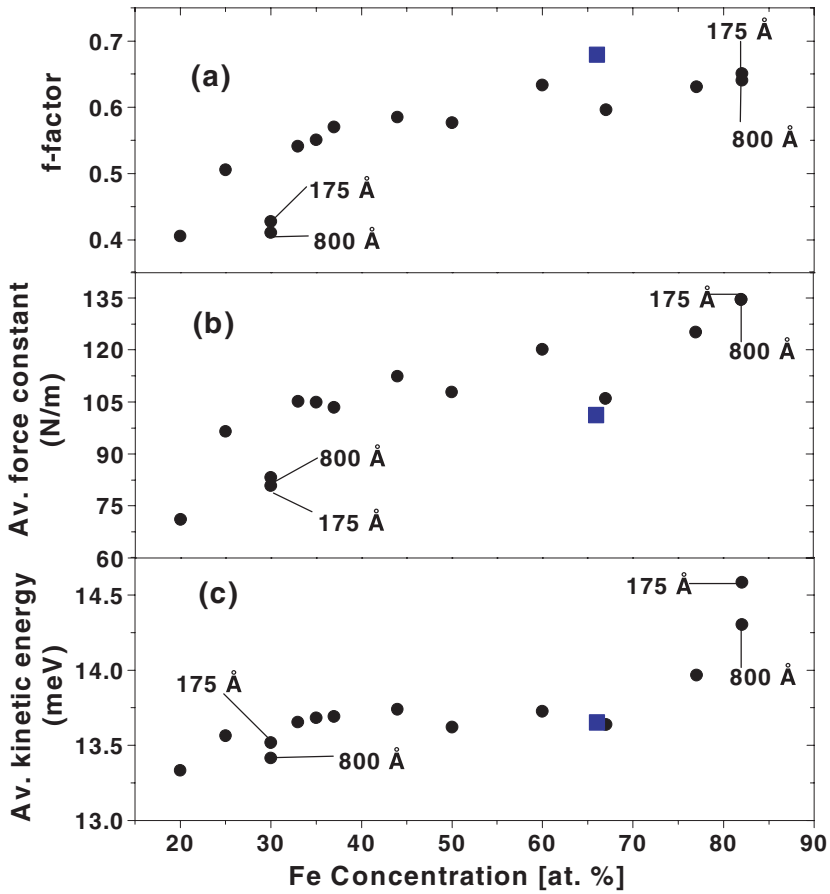

Figure 6. Probability for recoilless absorption (f factor) (a), average force constant (b) and average kinetic energy (c) versus Fe concentration for amorphous $Tb_{1-x}{}^{57}Fe_x$ thin films at 300 K (full circles). At 30 and 82 at.% different film thicknesses (17.5 and 80.0 nm, respectively) were studied. Values for the 80.0 thick epitaxial $Tb^{57}Fe_2(110)$ film at 300 K are also given (full squares).

$Tb^{57}Fe_2$ at 300 K are plotted in figure 5. Generally the two- and higher-order phonon contributions increase with decreasing f factor.

Figure 7 shows the partial VDOS, $g(E)$, of the epitaxial $Tb^{57}Fe_2(110)$ film and, for comparison, of the amorphous (a-)$Tb_{0.33}{}^{57}Fe_{0.67}$ film of the same composition. The measurements were performed at 300 and 10 K, respectively.

The partial VDOS of the crystalline $TbFe_2$ film is dominated by a strong sharp peak at 22 meV. There exists also a less intense sharp peak at 16 meV, and shoulders can be seen near ∼12 meV, ∼27 meV and possibly ∼32 meV for crystalline (c-)$TbFe_2$. These features essentially do not depend on the measurement temperature within the accuracy of the data; in fact, the $g(E)$ data at 300 and 10 K are remarkably similar. Since, to the best of our knowledge, no calculation of $g(E)$ for c-$TbFe_2$ is reported in the literature, we can only compare our result with experimental and computed $g(E)$ data of other rare-earth Laves phase compounds, such as $LaAl_2$ and $CeAl_2$ [36]. The comparison indicates that the main peak at 22 meV and the shoulders at higher energies arise from optical phonon modes, while the less intense peak at

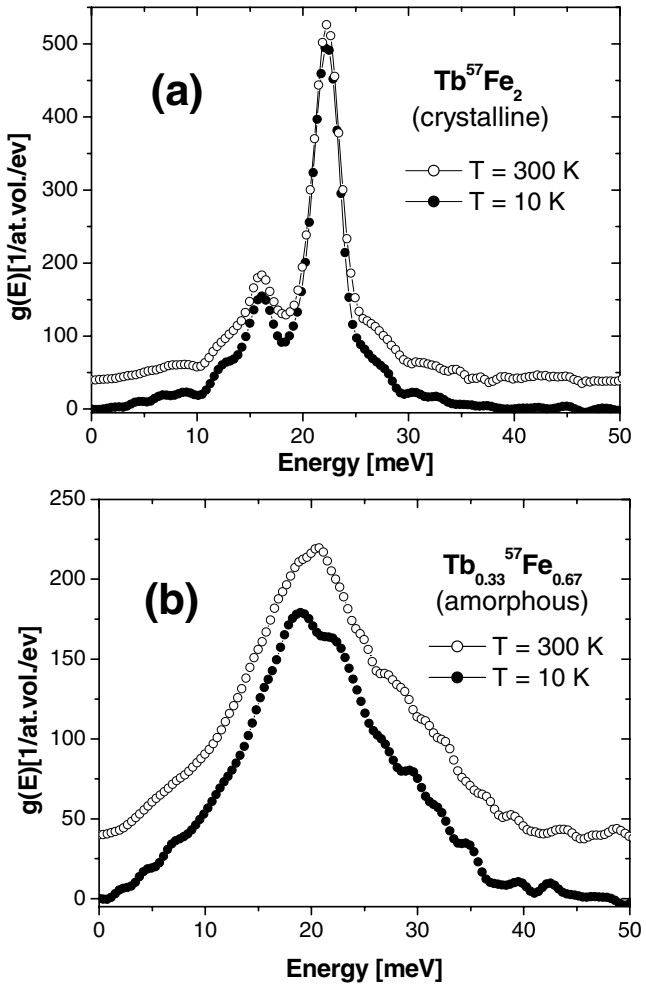

Figure 7. Partial VDOS, $g(E)$, of 80.0 nm thick epitaxial $Tb^{57}Fe_2(110)$ film (a) and 17.5 nm thick amorphous $Tb_{0.33}{}^{57}Fe_{0.67}$ film (b), measured at 300 K (open symbols) and 10 K (full symbols), respectively. Energy resolution: 2.3 meV. (For clarity the 300 K curves were displaced upwards by 40 (at. vol)$^{-1}$(eV)$^{-1}$ with respect to the 10 K curves.)

16 meV and the shoulders at lower energies originate from longitudinal and transverse acoustic phonon modes.

Contrary to c-$TbFe_2$, the partial VDOS of the a-$Tb_{0.33}{}^{57}Fe_{0.67}$ film (figure 7) represents a structureless broad feature, as anticipated for such an atomically disordered material, where van Hove singularities are smeared out. In the amorphous film distinct vibrational states like in the crystalline counterpart do not exist. It is interesting that similar effects have been found for phonons in nanocrystalline iron [37]. The maximum of $g(E)$ of the amorphous $Tb_{0.33}Fe_{0.67}$ film is located near $\sim$20 meV, i.e. between the distinct longitudinal and optical-mode features of the crystalline film. Moreover, the VDOS of a-$Tb_{0.33}Fe_{0.67}$ is enhanced at the low- and high-energy side relative to the VDOS of c-$TbFe_2$, and both VDOS curves extend to about the same maximum energy of about 40 meV (figure 7). The broad structureless VDOS of the amorphous material is a manifestation of a distribution of atomic force constants in the

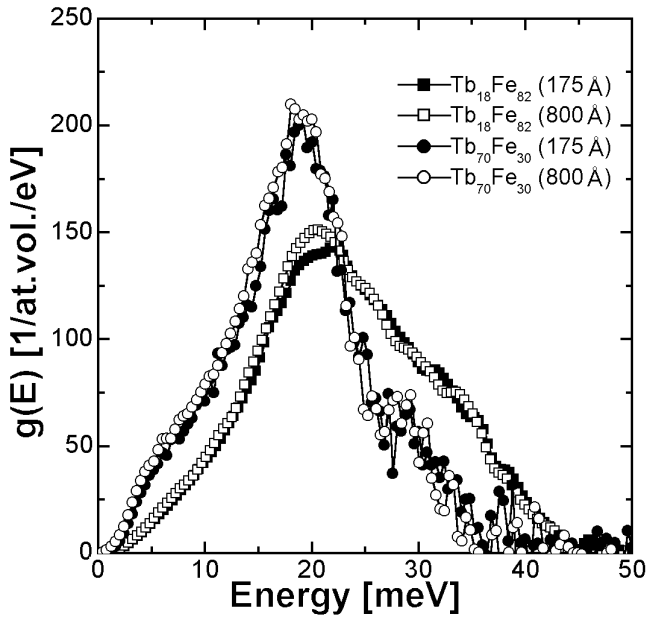

Figure 8. Partial VDOS, $g(E)$, of amorphous $Tb_{0.18}{}^{57}Fe_{0.82}$ (squares) and amorphous $Tb_{0.70}{}^{57}Fe_{0.30}$ (circles) thin films, both at 300 K. The film thickness t is 17.5 nm (full symbols) and 80.0 nm (open symbols), respectively. Energy resolution: 2.3 meV.

amorphous state. The additional intensity in the VDOS of the amorphous film (as compared to the crystalline case) above ∼30 meV (figure 7) may be attributed to vibrations of Fe atoms that are in regions of shorter distances to their neighbours (regions of positive internal pressure), as has been discussed for other binary amorphous alloys [38]. Qualitatively similar broad energy distributions (more exactly, generalized energy distributions) have been obtained by coherent inelastic neutron scattering on bulk samples of binary metallic glasses, e.g. a-$Mg_{70}Zn_{30}$ [38].

Similar to the crystalline case, the $g(E)$ data for a-$Tb_{0.33}Fe_{0.67}$ measured at 300 or 10 K essentially agree with each other (figure 7). Therefore, anharmonicity in the atomic potential is negligibly small in c-$TbFe_2$ and a-$Tb_{0.33}Fe_{0.67}$, contrary to bcc Fe [39]. We think that anharmonic effects, like phonon lifetime broadening, are of less importance for the VDOS of amorphous $Tb_{1-x}Fe_x$ alloy films, since we did not observe important differences at 300 and 10 K.

Concerning thin films, it is important to know whether their VDOS is thickness-dependent. For this purpose we have determined $g(E)$ of a-$Tb_{0.18}{}^{57}Fe_{0.82}$ and a-$Tb_{0.70}{}^{57}Fe_{0.30}$ films at 17.5 and 80.0 nm in thickness, as shown in figure 8. We do not observe drastic thickness effects in this thickness regime. Nevertheless, in the low-energy regime in figure 8 the data points (open symbols) of the thicker (80.0 nm) films can be seen to lie systematically slightly higher than the corresponding data points (full symbols) of the thinner films (17.5 nm). This effect results, for instance, in slightly smaller f factor values of the 80.0 nm thick films at 82 at.% Fe and 30 at.% Fe, as compared to 17.5 nm thick films (figure 6(a)).

Figure 9 represents a survey of the concentration dependence of the VDOS of various a-$Tb_{1-x}{}^{57}Fe_x$ thin films. There is a clear tendency that the main maximum of these structureless $g(E)$ curves as well as their maximum energy shift to lower energies with decreasing Fe content x, i.e. the Fe vibrations soften with decreasing x.

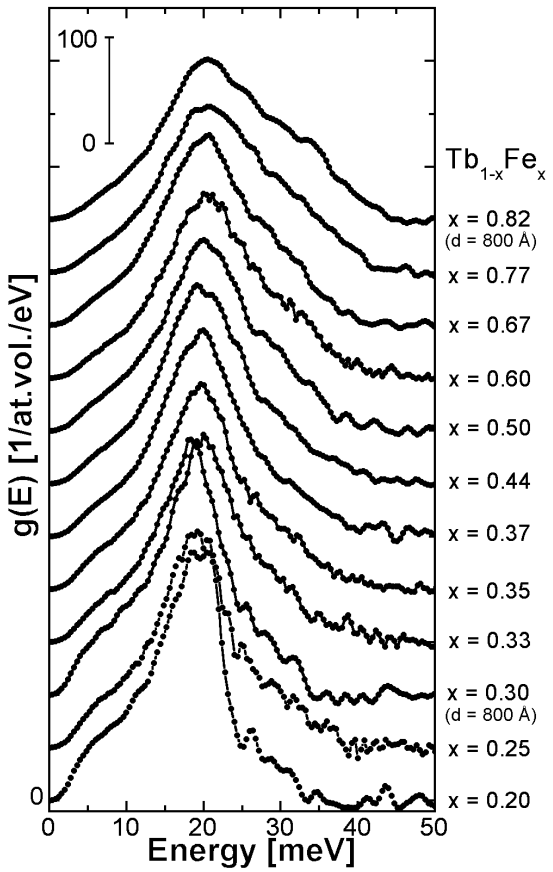

Figure 9. Partial VDOS, $g(E)$, of amorphous $Tb_{1-x}{}^{57}Fe_x$ thin films at 300 K for different compositions x. (For clarity, neighbouring curves are vertically displaced by 50 (at. vol)$^{-1}$ (eV)$^{-1}$). Energy resolution: 2.3 meV (from [11]).

4.3. Low-energy vibrational excitations

The low-energy modes in $g(E)$ of the amorphous films below ∼10 meV (figure 9) are of particular interest because of the boson-peak phenomenon [13–16]. The usual way to observe a deviation from Debye-like (E^2) behaviour is to plot the reduced VDOS, i.e. $g(E)/E^2$, versus E. In this representation strict Debye-like behaviour is reflected by a horizontal line which intersects the $g(E)/E^2$ axis at a value of $3V/[(2\pi)^{-2}h^3c_S^3]$, a value that is proportional to c_S^{-3} (c_S is the sound velocity and V is the volume of the unit cell) [5]. We like to emphasize that, for the crystalline $TbFe_2$ Laves phase, no van-Hove-type peaks in $g(E)$ exist below ∼10 meV according to figure 7.

In figure 10 we represent $g(E)/E^2$ versus E for our a-$Tb_{1-x}{}^{57}Fe_x$ thin film samples, as obtained from figure 9. A striking and unambiguous rise in $g(E)/E^2$ up to about 2.75 (at. vol)$^{-1}$ (eV)$^{-1}$ (meV)$^{-2}$ below ∼10 meV is observed for the Tb-richest a-$Tb_{0.80}{}^{57}Fe_{0.20}$ film. Further, a peak near 3 meV seems to exist for this sample; however, because of the limited energy resolution of 2.3 meV (FWHM) it is not clear at present whether this peak is real or an artefact of the NRIXS raw data evaluation, which includes subtraction of the elastic peak. (At 3.5 meV there is an about 10% contribution of the wing of the elastic

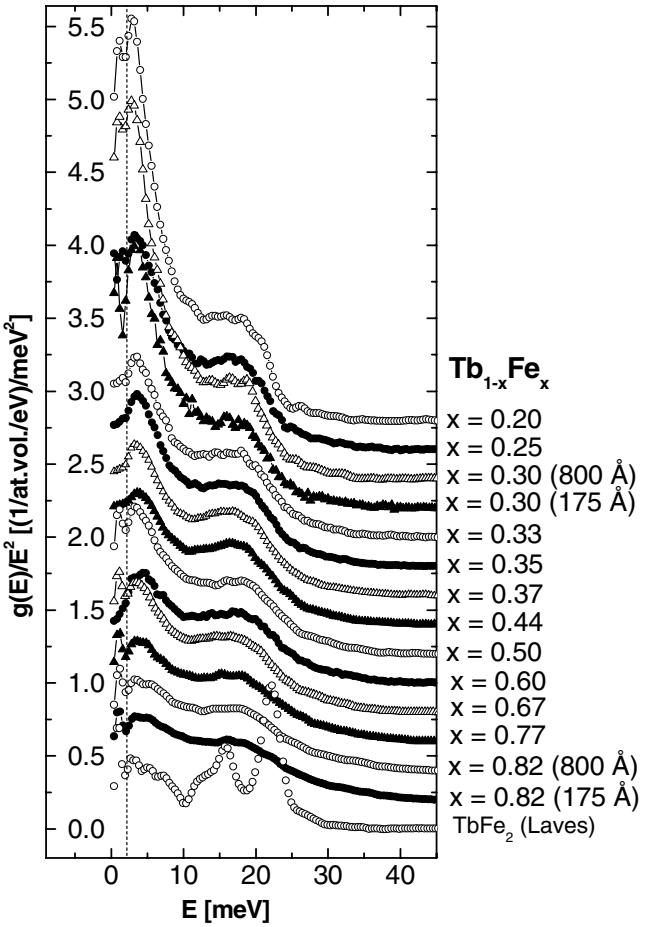

Figure 10. Reduced partial VDOS, $g(E)/E^2$, versus energy, E, of amorphous $Tb_{1-x}{}^{57}Fe_x$ thin film alloys of different composition x at 300 K, and of epitaxial $Tb^{57}Fe_2(110)$ thin film (Laves phase) at 300 K. (For clarity neighbouring spectra are vertically displaced by 0.2 (at. vol)$^{-1}$(eV)$^{-1}$(meV)$^{-2}$.) (The vertical dotted line indicates the FWHM of 2.3 meV of the instrumental resolution function. Data points below $E = 2.3$ meV are physically irrelevant.)

peak to the measured NRIXS intensity; at 4 meV this contribution is practically zero.) For the less Tb-containing amorphous films the rise in $g(E)/E^2$ below ∼10 meV is systematically weaker than for the Tb-richer samples, e.g. up to only ∼0.9 (at. vol)$^{-1}$ (eV)$^{-1}$ (meV)$^{-2}$ for a-$Tb_{0.33}{}^{57}Fe_{0.67}$. Again one can argue whether the peaks observed near 3 meV are real or an artefact. (The 'peaks' in several $g(E)/E^2$ curves below 2.5 meV in figure 10 are certainly artefacts of the elastic-peak subtraction technique combined with the limited energy resolution.)

In contrast, according to figure 10 the crystalline $Tb^{57}Fe_2$ film shows a much smaller $g(E)/E^2$ value of ∼0.5 (at. vol)$^{-1}$ (eV)$^{-1}$ (meV)$^{-2}$ near ∼3 meV than the amorphous films, in particular in comparison to the a-$Tb_{0.33}{}^{57}Fe_{0.67}$ film with the same composition. (The peaks at ∼22.5 and ∼16 meV for crystalline $Tb^{57}Fe_2$ result from the extrema in the VDOS due to optical and acoustic phonons of the cubic Laves phase (figure 7) and are *not* related to low-energy excitations leading to a boson peak.) Debye-like behaviour seems to occur below ∼5 meV in cubic $TbFe_2$. For comparison, Debye-like behaviour in bulk bcc Fe is observed in $g(E)/E^2$ below ∼15 meV with $g(E)/E^2 \approx 0.13$ (at. vol)$^{-1}$ (eV)$^{-1}$ (meV)$^{-2}$ [11].

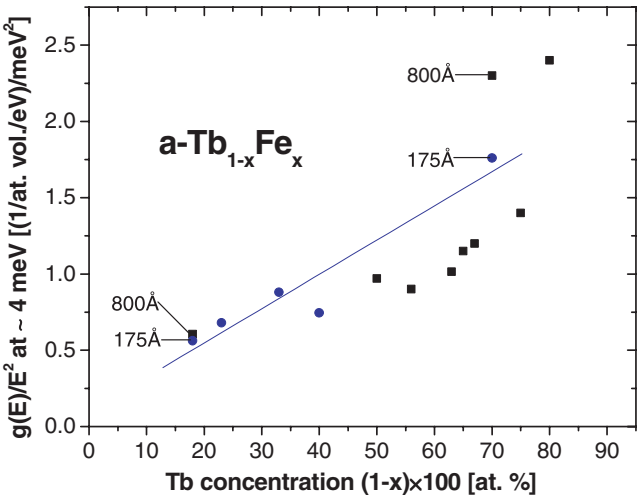

Figure 11. $g(E)/E^2$ at $E = 4$ meV (obtained from figure 10) versus Tb concentration $(1-x)100$ in a-$Tb_{1-x}{}^{57}Fe_x$ films. Full squares: for film thicknesses according to table 1 (except 17.5 nm). Full circles: for film thickness of 17.5 nm (the straight line is a least-squares fit to these data points).

Although we cannot claim that we have observed the full boson peak, figure 10 clearly proves the existence of non-Debye-like vibrational excitations below about 10 meV in quench-condensed a-$Tb_{1-x}{}^{57}Fe_x$ alloy films. They are not observed in crystalline systems such as cubic $TbFe_2$ and bcc Fe. The probability of excitation of these anomalous atomic vibrations increases with decreasing excitation energy and rising Tb content. Figure 11 exhibits the dependence of the $g(E)/E^2$ value at ∼4 meV (where artefacts can be excluded) on the Tb content $(1-x)$. At 18 at.% Tb the two data points (17.5 and 80.0 nm) are close together, but at 70 at.% Tb the corresponding two data points (17.5 and 80.0 nm) are clearly far apart. The film thickness appears to affect the low-energy excitations more at higher (70 at.%) than at lower (18 at.%) Tb concentration. Moreover, there is a considerable scatter of the data points above 70 at.% Tb in figure 11, analogous to that observed in figure 6. As mentioned before, these data fluctuations are possibly related to the eutectic point in the Tb–Fe phase diagram in that concentration regime. Considering the *same* film thickness of 17.5 nm, the data in figure 11 (full circles) provide evidence for an approximately linear relationship between the low-energy excitation probability and the Tb concentration in a-$Tb_{1-x}{}^{57}Fe_x$ alloy films, with a slope of 0.0225 ((at. vol)$^{-1}$(eV)$^{-1}$ (meV)$^{-2}$)/(at.% Tb). We should mention that we have observed very similar phenomena also in a-$Y_{1-x}{}^{57}Fe_x$ alloy films [40].

The microscopic origin of the observed anomalous low-energy excitations is still a matter of discussion. For metallic glasses, either vibrations of atoms on the surface of very small voids or oscillations in lower-density 'defect' regions of the metallic glass have been suggested [37] as possible explanations for low-energy excitations in these systems. We suggest that the larger atomic diameter of Tb (3.52 Å) as compared to that of Fe (2.48 Å) might be an important factor in the a-$Tb_{1-x}Fe_x$ system. In the structurally disordered network of large Tb atoms in Tb-rich amorphous alloys voids on an atomic scale might exist, which, when occupied by Fe atoms, provide enough space for the smaller Fe atoms to vibrate in shallow potentials with low frequencies. Such voids do not exist in crystalline systems. Figure 11 suggests that the density of such voids in a-$Tb_{1-x}{}^{57}Fe_x$ films might increase linearly with the Tb content.

5. Summary

The Fe-projected (partial) VDOS, $g(E)$, in vapour-quenched amorphous $Tb_{1-x}{}^{57}Fe_x$ thin film alloys ($0.20 \leqslant x \leqslant 0.82$) and, for comparison, in an epitaxial $Tb^{57}Fe_2(110)$ film (cubic Laves phase) was measured by NRIXS of 14.4125 keV synchrotron radiation with 2.3 meV energy resolution. The amorphous or crystalline structure, respectively, of the films was confirmed by XRD and ^{57}Fe CEMS. From the normalized NRIXS spectra the Lamb–Mössbauer factor (f factor), the average atomic kinetic energy and the average atomic force constant of the Fe atoms were obtained as a function of composition x. With increasing Tb content, the decrease of the f factor and the overall behaviour of the VDOS indicate the tendency to vibrational softening. No evidence for anharmonic vibrational effects in the temperature range from 10 to 300 K has been found. A plot of $g(E)/E^2$ versus E proves the existence of non-Debye-like vibrational excitations below about 10 meV in the amorphous films, but not in the crystalline film. For a constant film thickness of 17.5 nm, the probability of excitation of these anomalous atomic vibrations of Fe was found to depend approximately linearly on the Tb content.

Our investigations demonstrate that the NRIXS technique has evolved into a powerful and, at present, unique technique for the investigation of the lattice dynamics in ^{57}Fe-containing thin films.

Acknowledgments

We are indebted to U v Hörsten (Duisburg) for the expert preparation of samples. Work at Duisburg was supported by the Deutsche Forschungsgemeinschaft (Ke 273/17-1 and GRK 277). Use of the APS was supported by the US Department of Energy, Basic Energy Sciences, Office of Sciences, under contract no W-31-109-Eng-38.

References

[1] Seto M, Yoda Y, Kikuta S, Zhang X W and Ando A 1995 *Phys. Rev. Lett.* **74** 3828
[2] Sturhahn W, Toellner T S, Alp E E, Zhang X W, Ando M, Yoda Y, Kikuta S, Seto M, Kimball C W and Dabrowski B 1995 *Phys. Rev. Lett.* **74** 3832
[3] Chumakov A I, Rüffer R, Grünsteudel H, Grünsteudel H F, Grübel G, Metge J, Leupold O and Goodwin H A 1995 *Europhys. Lett.* **30** 427
[4] Chumakov A I and Sturhahn W 1999 *Hyperfine Interact.* **123/124** 781
[5] Alp E E, Sturhahn W and Toellner T S 2001 *J. Phys.: Condens. Matter* **13** 7645
Alp E E, Sturhahn W and Toellner T S 2001 *Hyperfine Interact.* **135** 295
[6] Sturhahn W, Röhlsberger R, Alp E E, Ruckert T, Schrör H and Keune W 1999 *J. Magn. Magn. Mater.* **198/199** 590
[7] Keune W and Sturhahn W 1999 *Hyperfine Interact.* **123/124** 847
[8] Ruckert T, Keune W, Sturhahn W, Hu M Y, Sutter J P, Toellner T S and Alp E E 2000 *Hyperfine Interact.* **126** 363
[9] Roldan Cuenya B, Keune W, Sturhahn W, Toellner T S and Hu M Y 2001 *Phys. Rev.* B **64** 235321
[10] Ruckert T, Keune W, Sturhahn W and Alp E E 2002 *J. Magn. Magn. Mater.* **240** 562
[11] Ruckert T, Keune W, Sahoo B, Sturhahn W, Toellner T S, Alp E E and Röhlsberger R 2003 *Hyperfine Interact.* at press
[12] For a review see: Phillips W A (ed) 1981 *Amorphous Solids—Low Temperature Properties* (Berlin: Springer)
[13] See the article by Jäckle J 1981 *Amorphous Solids—Low Temperature Properties* ed W A Phillips (Berlin: Springer)
[14] Schirmacher W, Diezemann G and Ganter C 1998 *Phys. Rev. Lett.* **81** 136 and references therein
[15] Schirmacher W, Diezemann G and Ganter C 2000 *Physica* B **284–288** 1147
[16] Suck H-B and Rudin H 1983 *Glassy Metals II* (*Topics in Applied Physics vol 53*) ed H Beck and H-J Güntherodt (Berlin: Springer) p 217
[17] Ruckert T, Tappert F, Brand R A and Keune W 1997 *J. Magn. Magn. Mater.* **165** 411

[18] Heiman N and Lee K 1975 *Phys. Lett.* A **55** 297
[19] Heiman N, Lee K and Potter R J 1976 *J. Appl. Phys.* **47** 2634
Heiman N, Lee K and Potter R J 1976 *AIP Conf. Proc.* **29** 130
[20] Toellner T S 1996 *PhD Dissertation* Northwestern University, Evanston, IL
[21] Toellner T S 2000 *Hyperfine Interact.* **125** 3
[22] Baron A Q R 2000 *Hyperfine Interact.* **125** 29
[23] Sturhahn W 2000 *Hyperfine Interact.* **125** 149
[24] Röhlsberger R, Sturhahn W, Toellner T S, Quast K W, Hession P, Hu M, Sutter J and Alp E E 1999 *J. Appl. Phys.* **86** 584
[25] Oderno V, Dufour C, Dumesnil K, Mangin Ph and Marchal G 1996 *J. Cryst. Growth* **165** 175
[26] Brand R A 1987 *Nucl. Instrum. Methods* B **28** 398
[27] Mougin A, Dufour C, Dumesnil K and Mangin Ph 2000 *Phys. Rev.* B **62** 9517
[28] Eymery J P, Fnidiki A, Krishnan R, Tessier M and Vitton J P 1988 *Phys. Rev.* B **38** 11931
[29] Sturhahn W and Kohn V G 1999 *Hyperfine Interact.* **123/124** 367
[30] Lipkin H 1960 *Ann. Phys., NY* **9** 332
[31] Lipkin H 1986 *Quantum Mechanics* (Amsterdam: North-Holland)
[32] Lipkin H 1995 *Phys. Rev.* B **52** 10073
[33] Mofatt W G 1984 *The Handbook of Binary Phase Diagrams* vol 3 (Schenectady, NY: Genium)
[34] Chumakov A 1999 *Hyperfine Interact.* **124** 809
[35] Hu M *et al* 1999 *Nucl. Instrum. Methods* A **428** 551
[36] Kress W 1987 *Phonon Disperion Curves, One-Phonon Densities of States and Impurity Vibrations of Metallic Systems (PHYSICS DATA)* vol 26-1 (Karlsruhe, Germany: Fachinformationszentrum Karlsruhe) pp 173–5
[37] Fultz B, Ahn C C, Alp E E, Sturhahn W and Toellner T S 1997 *Phys. Rev. Lett.* **79** 937
[38] Suck H-B and Rudin H 1983 *Glassy Metals II* (*Topics in Applied Physics vol 53*) ed H Beck and H-J Güntherodt (Berlin: Springer) p 217
[39] Chumakov A I, Rüffer R, Baron A Q R, Grünsteudel H and Grünsteudel H F 1996 *Phys. Rev.* B **54** 1
[40] Sahoo B, Keune W, Ruckert T, Sturhahn W, Toellner T S and Alp E E, to be published